AIP Advances

Third-order accurate 13-moment equations for non-continuum transport phenomenon

Cite as: AIP Advances **13**, 045311 (2023); https://doi.org/10.1063/5.0143420
Submitted: 23 January 2023 • Accepted: 13 March 2023 • Published Online: 06 April 2023

Upendra Yadav, Anirudh Jonnalagadda and Amit Agrawal

Third-order accurate 13-moment equations for non-continuum transport phenomenon

Cite as: AIP Advances 13, 045311 (2023); doi: 10.1063/5.0143420
Submitted: 23 January 2023 • Accepted: 13 March 2023 •
Published Online: 6 April 2023

Upendra Yadav,[1,a] Anirudh Jonnalagadda,[2,b] and Amit Agrawal[1,c]

AFFILIATIONS

[1] Department of Mechanical Engineering, Indian Institute of Technology Bombay, Powai 400076, India
[2] Department of Computational and Data Sciences, Indian Institute of Science, Bengaluru, India

[a] upendra.yadav001@iitb.ac.in
[b] anirudhj@iisc.ac.in
[c] Author to whom correspondence should be addressed: amit.agrawal@iitb.ac.in

ABSTRACT

The derivation of analytical equations of non-continuum macroscopic transport phenomena is underpinned by approximate descriptions of the particle distribution function and is required due to the inability of the Navier–Stokes equations to describe flows at high Knudsen number ($Kn \sim 1$). In this paper, we present a compact representation of the second-order correction to the Maxwellian distribution function and 13-moment transport equations that contain fewer terms compared to available moment-based representations. The intrinsic inviscid and isentropic assumptions of the second-order accurate distribution function are then relaxed to present a third-order accurate representation of the distribution function, using which corresponding third-order accurate moment transport equations are derived. Validation studies performed for Grad's second problem and the force-driven plane Poiseuille flow problem at non-zero Knudsen numbers for Maxwell molecules highlight an improvement over results obtained by using the Navier–Stokes equations and Grad's 13-moment (G13) equations. To establish the ability of the proposed equations to accurately capture the bulk behavior of the fluid, the results of Grad's second problem have been validated against the analytical solution of the Boltzmann equation. For the planar Poiseuille flow problem, validations against the direct simulation Monte Carlo method data reveal that, in contrast to G13 equations, the proposed equations are capable of accurately capturing the Knudsen boundary layer.

I. INTRODUCTION

Several transport equations of varying degrees of accuracy and complexity have been derived by using approximations of the distribution function obtained through the Chapman–Enskog multi-scale expansion. Of these, the well-known Navier–Stokes (N–S) equations, which are the first-order approximation to the Boltzmann Equation, can be used in their original form only for the continuum flow regime where the Knudsen number, Kn, is less than 10^{-3}. However, there are several real-life problems where the flow variables can no longer be treated as continuum fields.[1–7] In such situations, the N–S equations need to be either augmented or abandoned altogether.

For flows in the slip flow regime $\left(10^{-3} < \mathrm{Kn} < 10^{-1}\right)$, the Knudsen number envelope of the N–S equations has been extended by providing modified descriptions of the velocity and temperature boundary conditions.[8–10] Nevertheless, despite incorporating these modifications, the N–S equations only capture weak non-equilibrium scenarios and lose their applicability beyond Kn greater than 10^{-2}.[11,12] As a result, various higher-order transport equations have been developed to account for the non-equilibrium effects for Kn greater than 10^{-1}. These higher-order transport equations can be broadly classified into distinct categories on account of the significantly different approaches adopted to construct the required distribution function:[10] the Burnett type equations[1,2] and moment method-based equations.[13,14] In this paper, we focus on moment method-based formulations.

The first category of higher-order transport equations, namely that of the Burnett-type equations, originated from the original Burnett equations,[15] which make use of the second-order approximation of the distribution function obtained from the Chapman–Enskog expansion to present non-linear constitutive

relationships for the stress tensor and heat flux vector. The second-order distribution function used to derive the original Burnett equations contained material derivatives of the field variables,[1] presented an alternate form, namely the Conventional Burnett equations, wherein the material derivatives were replaced by the spatial gradients described by the Euler equations. To improve the order of accuracy of second-order Burnett equations, an $\mathcal{O}(\mathrm{Kn}^3)$ set of equations, namely the super-Burnett equations,[16] was obtained to avoid the inviscid and isentropic assumptions associated with the Euler equations. To address the stability concerns associated with the original, conventional, and super-Burnett[17] equations, Zhong, MacCormack, and Chapman[18] derived the augmented Burnett equations by introducing certain super-Burnett terms into the original Burnett equations. It is also important to emphasize that the augmented Burnett equations and, indeed, the original Burnett and super-Burnett equations were found to violate the H-theorem,[19] a kinetic equivalent of the Second Law of Thermodynamics. However, the BGK-Burnett equations[20,21] were found to provide stable, H-Theorem consistent numerical solutions albeit at the cost of recovering a nonphysical unit Prandtl number.[22] Despite significantly contributing to scientific understanding, the above-mentioned equations are associated with several drawbacks. Therefore, apart from the Burnett variants mentioned earlier, thermomechanically consistent Burnett,[23] simplified Burnett,[24] and reduced Burnett[25] equations have also been presented.

Moment-based higher-order transport equations were proposed by Grad[13] as a simpler alternative to Burnett-type equations. The well-known, linearly stable Grad's 13-moment, or G13, equations were derived by expressing the distribution function in terms of a Hermite polynomial expansion with the macroscopic hydrodynamics being obtained by taking moments of the Boltzmann equation. However, in contrast to Burnett-type equations, the stress tensor and heat flux vector in the momentum and energy equations, respectively, were retained as primary variables in addition to density, velocity, and temperature in the moment-based approach, with separate evolution equations being prescribed to describe their dynamics.

The G13 equations have demonstrated the ability to capture several rarefied phenomena,[10,26–28] which elude the N–S equations. However, it is noteworthy that the G13 equations have been successfully applied to only a few boundary value problems[29] as they fail to capture the boundary layer[10] and produce discontinuous shock structures for Mach numbers ≥1.65 due to their symmetric hyperbolic nature.[14,30] These limitations prompted the development of $\mathcal{O}(\mathrm{Kn}^3)$ accurate regularized 13-moment or R13 equations that use a regularization method to correct the G13 equations by incorporating correction terms taken from the super-Burnett equations.[31,32] Furthermore, in order to push the parameter range for which accurate results can be obtained,[33] proposed fifth-order regularized 26-moments, or R26, equations by expanding the set of primary variables from 13 to 26. Due to the modifications introduced, both the R13 and R26 equations successfully predicted several critical rarefied phenomena, which are, otherwise, beyond the scope of the N–S, Burnett, and G13 equations.[33–35] In contrast, the recent work by Singh and Agrawal[36] adopts a non-equilibrium thermodynamics approach to present an Onsager-reciprocity-principle-consistent representation of the distribution function and further obtain the Onsager-13 (or O13)-moment equations[36] and Onsager-Burnett (or OBurnett) equations.[37] Note that both the O13 and OBurnett formulations are $\mathcal{O}(\mathrm{Kn}^2)$, i.e., second-order accurate in Knudsen number.

In this paper, we prescribe a simpler representation of the second-order correction to the Maxwellian distribution function, which has fewer terms in comparison to that reported by Singh and Agrawal.[36] Furthermore, we also construct an enhanced representation of the distribution function that includes third-order $\mathcal{O}(\mathrm{Kn}^3)$ accurate terms. Thereafter, we use these representations to obtain sets of moment-type higher-order transport equations having second- and third-order accuracy. Note that the proposed second-order moment equations yield the same behavior as the equations proposed by Singh and Agrawal,[36] albeit with fewer terms due to the compact nature of the second-order representation of the distribution function, while the newly proposed third-order accurate moment equations present an alternative to the R13 equations. However, the proposed equations lack linear terms of the super-Burnett order, which were previously shown to be necessary for accurately capturing the Knudsen layer in wall-bounded rarefied flows.[32] Thus, we also present a modified version of the proposed set of equations that include linear terms of the second order.

The rest of this paper is laid out as follows: In Secs. II and III, a systematic derivation of the two forms of the distribution function and the second- and third-order accurate 13-moment equation is presented. Thereafter, in Sec. IV, we present the modified set of equations that have linear contributions of the second order. Section V presents a validation of the proposed equations by solving two benchmark problems: Grad's second and plane Poiseuille flow problem. Moreover, we also proved that the present equations are consistent with the second law of thermodynamics for the same two problems. Finally, in Sec. VI, we discuss the salient features of the proposed equations, contrast them with the existing G13 equations, and conclude this paper in Sec. VII.

II. DERIVATION OF THE DISTRIBUTION FUNCTION

The kinetic theory description of the evolution of thermodynamic systems comprising dilute gases is given by the well-known Boltzmann equation,

$$\frac{\partial f}{\partial t} + \frac{\partial}{\partial \boldsymbol{x}} \cdot (\boldsymbol{c} f) = \mathcal{J}(f, f), \tag{1}$$

where $f = f(\boldsymbol{x}, \boldsymbol{c}, t)$, with $\boldsymbol{x}$, $\boldsymbol{c}$, and t being the position vector, molecular velocity, and time, respectively, is the single-particle distribution function, and $\mathcal{J}(f, f)$ represents the integro-differential binary collision operator. The solution of Eq. (1) yields the single-particle distribution function, which represents the probability of finding a particle in a very small region of the phase space. Furthermore, by evaluating the moments of the distribution function, macroscopic conserved variables, i.e., the mass, momentum, and energy density, along with stress tensor and heat flux vector, can be obtained. Therefore, the distribution function, which acts as an interlink between the microscopic and macroscopic description of the flow processes, is an essential quantity for understanding the physics of rarefied gas flows.[1–4,38]

The first step in deriving any set of hydrodynamic governing equations is to obtain the state of gas by specifying the approximate form of the distribution function, $f(\boldsymbol{x}, \boldsymbol{c}, t) \approx f_n(\boldsymbol{x}, \boldsymbol{c}, t)$, where n is

the desired level of approximation. The zeroth-order approximation corresponds to the simplest case of gas at equilibrium for which the three-dimensional distribution function for a monatomic gas is given by the Maxwellian,[39]

$$f \approx f_0(\boldsymbol{x}, \boldsymbol{c}, t) = \frac{\rho}{m}\left(\frac{\beta}{\pi}\right)^{(3/2)} \exp\left[-\beta(|\boldsymbol{c}-\boldsymbol{u}|)^2\right], \tag{2}$$

where $\rho(\boldsymbol{x}, t)$ and $\boldsymbol{u}(\boldsymbol{x}, t)$ are the bulk density and velocity, respectively, m is the molecular mass, and $\beta = 1/(2\mathrm{RT})$, with R and $T(\boldsymbol{x}, t)$ being the specific gas constant and absolute temperature, respectively. For collision invariant quantities represented by the set $\Psi = \left\{1, \boldsymbol{c}, \frac{\boldsymbol{c}^2}{2}\right\}$, physically observed bulk macroscopic fields are obtained as moments of f_0,

$$\langle \Psi, f_0 \rangle = \int m\ \Psi\ f_0\ d\boldsymbol{c} = \left\{\rho, \rho\boldsymbol{u}, \frac{3}{2}\rho RT\right\}. \tag{3}$$

At the first order of approximation, a Chapman–Enskog expansion of the Boltzmann equation yields the distribution function as a correction to the Maxwellian $\left(\tilde{f}_1^{\,(CE)}\right)$ as[1]

$$f \approx f_1 = f_0 - \underbrace{\frac{f_0}{\tilde{\nu}}\left\{\left(\frac{\boldsymbol{C}^2}{2R} - \frac{5}{2}\right)(\boldsymbol{C}\cdot\nabla(\ln\ T)) + \frac{1}{R}\left[\left(\boldsymbol{C}\otimes\boldsymbol{C} - \frac{1}{3}\mathbf{C}^2\delta\right) : (\nabla\otimes\boldsymbol{u})\right]\right\}}_{\tilde{f}_1^{\,(CE)}}, \tag{4}$$

where $1/\tilde{\nu}$ $(= \mu/p)$ is the relaxation time with which the system reaches the equilibrium state, $\boldsymbol{C} = (\boldsymbol{c} - \boldsymbol{u})$ is the peculiar velocity, and $\otimes$ denotes the outer product.

From an alternate non-equilibrium thermodynamics perspective, the distribution function can be expressed in terms of thermodynamic forces and corresponding microscopic conjugate fluxes, $\boldsymbol{X_j}$ and $\boldsymbol{\Upsilon_j}$, associated with the jth non-equilibrium process of the system.[40,41] In particular, the first-order approximation of the distribution function can be obtained through an iterative refinement as[42]

$$f_1 = f_0 - \underbrace{\sum_j \boldsymbol{\Upsilon_j} \odot \boldsymbol{X_j}}_{\tilde{f}_1}, \tag{5}$$

where $\tilde{f}_1$ is the correction to the Maxwellian and

$$\boldsymbol{\Upsilon_j} \odot \boldsymbol{X_j} = t_{r(j)}\left[\frac{\partial f_0}{\partial t} + \frac{\partial}{\partial x_j}(c_j f_0)\right]_{X_j=0\ \forall\, j\neq i}, \tag{6}$$

where the symbol $\odot$ represents a full tensorial contraction that is non-zero for tensors of the same order and $t_{r(j)}$ represents the relaxation time associated with the jth process. Here, it is important to note that the formulation presented in Eq. (6) is consistent with the Onsager Symmetry Principle and is, therefore, also consistent with the H-Theorem. Upon simplifying Eq. (6), the first-order correction to f_0 is obtained in terms of destabilizing viscous and thermal non-equilibrium processes, which are, henceforth, denoted by the subscripts τ and q, respectively. Explicitly, the thermodynamic forces $(\boldsymbol{X}_\tau, \boldsymbol{X}_q)$ and associated conjugate fluxes $(\boldsymbol{\Upsilon_\tau}, \boldsymbol{\Upsilon_q})$ are given as[42]

$$\boldsymbol{\Upsilon}_i = -f_0\, t_{r(i)}\, \tilde{\boldsymbol{\Upsilon}}_i, \text{ with } i \in \{\tau, q\}, \tag{7a}$$

where

$$\tilde{\boldsymbol{\Upsilon}}_\tau = -\left[\boldsymbol{C}\otimes\boldsymbol{C} - \frac{1}{3}|\boldsymbol{C}|^2\boldsymbol{\delta}\right], \tag{7b}$$

$$\tilde{\boldsymbol{\Upsilon}}_q = -\left(\frac{5}{2\beta} - |\boldsymbol{C}|^2\right)\boldsymbol{C}, \tag{7c}$$

and

$$\boldsymbol{X}_\tau = \beta\left[\nabla\otimes\boldsymbol{u} + (\nabla\otimes\boldsymbol{u})^T\right], \tag{7d}$$

$$\boldsymbol{X}_q = \nabla\beta, \tag{7e}$$

where $\boldsymbol{\delta}$ represents the Kronecker delta. It should be noted that Eq. (7a) incorporates two different relaxation times for momentum transport $\left(t_{r(\tau)} = \mu/p\right)$ and energy transport $\left(t_{r(q)} = \kappa(\gamma-1)/(R\gamma p) = t_{r(\tau)}/\mathrm{Pr}\right)$, where μ and p represent the dynamic viscosity and pressure, while γ and κ represent the adiabatic index and thermal conductivity, respectively; by suitably choosing the values of the two relaxation times, a physically consistent Prandtl number, Pr, value can be obtained. Furthermore, the dynamic viscosity and thermal conductivity are assumed to be temperature-dependent functions of the form $\mu = \mu_0(T/T_0)^\varphi$ and $\kappa = \kappa_0(T/T_0)^\varphi$, respectively, where μ_0 and κ_0 are the dynamic viscosity and thermal conductivity evaluated at a reference temperature T_0, and φ is the interaction potential between the two molecules. Here, it is noteworthy that the temperature-dependent transport coefficients μ and κ ensure a temperature-dependent variation of the momentum and thermal diffusion time scales. Furthermore, it can be easily established that Eq. (4) is retrieved from Eq. (5) upon using $t_{r(\tau)} = t_{r(q)} = (1/\tilde{\nu})$.[43]

To ensure the conservation of mass, momentum, and energy, each higher-order correction to the distribution function $(\tilde{f}_i)$ is required to satisfy the property of additive invariance,[37,44]

$$\langle \Psi, \tilde{f}_i \rangle = 0. \tag{8}$$

It should be noted that Eqs. (3) and (8) are together called compatibility conditions. The first-order correction to the distribution function, i.e., $\tilde{f}_1$ from Eq. (5), can be shown to satisfy the additive invariance condition.[10]

The second-order approximation of the distribution function, f_2, can be derived by extending Eq. (5) as[10,36,37,42,45,46]

$$f_2 = f_1 + \underbrace{\sum_{k,j}(\boldsymbol{\Upsilon}_{kj}\odot\boldsymbol{X}_k)\odot\boldsymbol{X}_j}_{\tilde{f}_2}, \tag{9}$$

where f_1 has been presented earlier in Eq. (5) and $\tilde{f}_2$ is the second-order correction with $(\Upsilon_{kj} \odot \boldsymbol{X}_k)$ being[10,36,47]

$$\Upsilon_{kj} \odot \boldsymbol{X}_k = t_{r(j)} \left[\frac{\partial \Upsilon_j}{\partial t} + \frac{\partial (c_k \Upsilon_j)}{\partial x_k} \right]_{X_j = 0 \ \forall \, j \neq i}. \tag{10}$$

Analogous to Eq. (5), the construction of Eq. (9) is also compliant with Onsager's symmetry principle.[36,42] Furthermore, like Eq. (6), the tensorial contraction in Eq. (9) vanishes for tensors of different orders.[36,42,48]

To construct the required higher-order distribution function, we first rewrite Eq. (10) in terms of material derivatives as follows:

$$\Upsilon_{kj} \odot \boldsymbol{X}_k = t_{r(j)} \left[\frac{D \Upsilon_j}{Dt} + C_k \frac{\partial \Upsilon_j}{\partial x_k} \right]_{X_j = 0, \ \forall \, j \neq i}, \tag{11}$$

where D/Dt denotes the material derivative, and C_k is the peculiar velocity defined earlier. The material derivatives present in Eq. (11) can be replaced by using either Euler or N–S equations. In Sec. II A, we revisit the formulation presented by Singh and Agrawal[36] that was derived by using the Euler equation substitutions to present a simpler form of the distribution function having fewer terms. It should be remarked that, while using the Euler equations yields $\mathcal{O}(\mathrm{Kn}^2)$ accurate higher-order transport equations, the inviscid and isentropic assumptions associated with the Euler equations do not hold for rarefied gas flow problems.[49] Here, we follow the approach used by Balakrishnan, Agarwal, and Yun,[44] where the N–S equations were incorporated into the Chapman–Enskog expansion procedure to obtain an $\mathcal{O}(\mathrm{Kn}^3)$ representation of the Bhatnagar–Gross–Krook (BGK)-Burnett equations and present $\mathcal{O}(\mathrm{Kn}^3)$ second-order correction of f_2 in Sec. II B.

A. Second-order accurate distribution function

Upon substituting the definitions of the microscopic flux from Eqs. (7a)–(7c) into Eq. (11) and replacing the material derivatives with expressions from the Euler equations, we obtain the second-order correction terms as

$$\Upsilon_{\tau\tau} \odot \boldsymbol{X}_\tau = t^2_{r(\tau)} f_0 \Bigg\{ \underbrace{-C_l \left[C_i \frac{\partial u_j}{\partial x_l} + \left(C_j \frac{\partial u_i}{\partial x_l} \right)^T \right]}_{\omega_1} + \underbrace{\frac{1}{2\beta} \left[C_i \frac{\partial g}{\partial x_j} + \left(C_j \frac{\partial g}{\partial x_i} \right)^T \right]}_{\omega_2}$$
$$- \left[\underbrace{\frac{1}{3\beta} C_k \frac{\partial g}{\partial x_k}}_{\omega_3} - \underbrace{\frac{1}{3\beta} (\boldsymbol{C} \otimes \boldsymbol{C}) : \boldsymbol{X}_\tau}_{\omega_4} \right] \delta_{ij} + \tilde{\Upsilon}_\tau \left[\underbrace{\tilde{\Upsilon}_\tau : \boldsymbol{X}_\tau}_{\omega_5} + \underbrace{\tilde{\Upsilon}_q \cdot \boldsymbol{X}_q}_{\omega_6} \right]$$
$$+ \tilde{\Upsilon}_\tau \left[\underbrace{\frac{2\varphi - 5}{3} \frac{\partial u_l}{\partial x_l}}_{\omega_7} + \underbrace{\frac{\varphi}{\beta} C_l \frac{\partial \beta}{\partial x_l}}_{\omega_8} + \underbrace{C_l \frac{\partial g}{\partial x_l}}_{\omega_9} \right] \Bigg\}, \tag{12}$$

$$\Upsilon_{qq} \odot \boldsymbol{X}_q = t^2_{r(q)} f_o \Bigg\{ \underbrace{\tilde{\Upsilon}_q \left[\tilde{\Upsilon}_\tau : \boldsymbol{X}_\tau + \tilde{\Upsilon}_q \cdot \boldsymbol{X}_q \right]}_{\xi_1} - C_i \left[\underbrace{\frac{1}{\beta} C_l \frac{\partial g}{\partial x_l}}_{\xi_2} - \underbrace{\frac{1}{\beta} (\boldsymbol{C} \otimes \boldsymbol{C}) : \boldsymbol{X}_\tau}_{\xi_3} \right]$$
$$- C_i \left[\underbrace{\frac{5}{3\beta} \frac{\partial u_k}{\partial x_k}}_{\xi_4} + \underbrace{\frac{5}{2\beta^2} C_l \frac{\partial \beta}{\partial x_l}}_{\xi_5} \right] + \left(\frac{5}{2\beta} - |C|^2 \right) \left[\underbrace{\frac{1}{2\beta} \frac{\partial g}{\partial x_i}}_{\xi_6} - \underbrace{C_l \frac{\partial u_i}{\partial x_l}}_{\xi_7} \right]$$
$$+ \tilde{\Upsilon}_q \left[\underbrace{\frac{2\varphi - 5}{3} \frac{\partial u_l}{\partial x_l}}_{\xi_8} + \underbrace{\frac{\varphi}{\beta} C_l \frac{\partial \beta}{\partial x_l}}_{\xi_9} + \underbrace{C_l \frac{\partial g}{\partial x_l}}_{\xi_{10}} \right] \Bigg\}, \tag{13}$$

where $g = \ln(\rho/\beta)$.

Upon checking if $\tilde{f}_2$ satisfies the additive invariance property, in line with the results reported in Singh and Agrawal,[36] we find that only the condition $\langle 1, \tilde{f}_2 \rangle = 0$ corresponding to the conservation of mass is satisfied. Thus, it is necessary to modify Eqs. (12) and (13) such that all three compatibility conditions are satisfied without breaking Onsager's symmetry principle. To achieve this goal, we follow the procedure laid out

by Balakrishnan, Agarwal, and Yun[44] and Agarwal, Yun, and Balakrishnan.[22]

First, we represent $\langle \Psi, \tilde{f}_2 \rangle$ explicitly in terms of Eqs. (12) and (13) as follows:

$$\langle \Psi, \tilde{f}_2 \rangle = t^2_{r(\tau)} \left(\sum_{i=1}^{9} \langle \Psi, f_0 \omega_i \rangle \right) \odot \boldsymbol{X}_\tau + t^2_{r(q)} \left(\sum_{i=1}^{10} \langle \Psi, f_0 \xi_i \rangle \right) \odot \boldsymbol{X}_q, \tag{14}$$

where the running index i represents each term appearing in Eqs. (12) and (13). Thereafter, in order to make $\left\langle \left\{ \boldsymbol{c}, \frac{\boldsymbol{C}^2}{2} \right\}, \tilde{f}_2 \right\rangle$ identically equal to zero, we introduce corrections to modify Eqs. (12) and (13), respectively, as follows:

$$\langle \boldsymbol{c}, \tilde{f}_2 \rangle + t^2_{r(\tau)} \left(\sum_{i=1}^{9} \alpha_i \langle c_i, f_0 \omega_i \rangle \right) \odot \boldsymbol{X}_\tau + t^2_{r(q)} \left(\sum_{i=1}^{10} \beta_i \langle c_i, f_0 \xi_i \rangle \right) \odot \boldsymbol{X}_q = 0 \tag{15}$$

and

$$\left\langle \frac{|\boldsymbol{C}|^2}{2}, \tilde{f}_2 \right\rangle + t^2_{r(\tau)} \left(\sum_{i=1}^{9} \alpha_i \left\langle \frac{|\boldsymbol{C}|^2}{2}, f_0 \omega_i \right\rangle \right) \odot \boldsymbol{X}_\tau + t^2_{r(q)} \left(\sum_{i=1}^{10} \beta_i \left\langle \frac{|\boldsymbol{C}|^2}{2}, f_0 \xi_i \right\rangle \right) \odot \boldsymbol{X}_q = 0 \tag{16}$$

where α_i and β_i are real-valued unknown correction coefficients. Equations (15) and (16) form an under-determined system of equations for which one possible solution is presented by the following values of α_i and β_i:

$$\alpha_i = \begin{cases} -1, & \text{if } i = 1, 4, 5, \\ -\left(1 + \frac{1}{\varphi}\right), & \text{if } i = 7, \\ 0, & \text{otherwise}, \end{cases} \tag{17}$$

and

$$\beta_i = \begin{cases} -\left(1 + \frac{2}{\varphi}\right), & \text{if } i = 9, \\ 0, & \text{otherwise}. \end{cases} \tag{18}$$

With these modifications, we can represent the second-order accurate distribution function as

$$f_2^{\mathcal{O}(\mathrm{Kn}^2)} = f_0 - \sum_j \boldsymbol{\Upsilon}_j \odot \boldsymbol{X_j} + \sum_{k,j} (\boldsymbol{\Upsilon}'_{kj} \odot \boldsymbol{X}_k) \odot \boldsymbol{X}_j, \tag{19}$$

where

$$\begin{aligned} (\boldsymbol{\Upsilon}'_{\tau\tau} \odot \boldsymbol{X}_\tau) = (\boldsymbol{\Upsilon}_{\tau\tau} \odot \boldsymbol{X}_\tau) + t^2_{r(\tau)} f_0 \\ \times \left\{ \begin{array}{r} C_l \left[C_i \frac{\partial u_j}{\partial x_l} + \left(C_j \frac{\partial u_i}{\partial x_l} \right)^T \right] - \left[\frac{1}{3\beta} (\boldsymbol{C} \otimes \boldsymbol{C}) : \boldsymbol{X}_\tau \right] \delta_{ij} \\ -\tilde{\boldsymbol{\Upsilon}}_\tau (\tilde{\boldsymbol{\Upsilon}}_\tau : \boldsymbol{X}_\tau) - \left(1 + \frac{1}{\varphi}\right) \tilde{\boldsymbol{\Upsilon}}_\tau \left(\frac{\varphi}{\beta} C_l \frac{\partial \beta}{\partial x_l} \right) \end{array} \right\} \end{aligned} \tag{20}$$

and

$$(\boldsymbol{\Upsilon}'_{qq} \odot \boldsymbol{X}_q) = (\boldsymbol{\Upsilon}_{qq} \odot \boldsymbol{X}_q) + t^2_{r(q)} f_0 \left\{ -\left(1 + \frac{2}{\varphi}\right) \tilde{\boldsymbol{\Upsilon}}_q \frac{\varphi}{\beta} C_l \frac{\partial \beta}{\partial x_l} \right\}. \tag{21}$$

B. Third-order accurate distribution function

Building on the analysis presented in Sec. II A, we now replace the material derivative in Eq. (11) with the N–S equations. Such a substitution incorporates additional non-linear terms comprising the deviatoric viscous stress tensor (σ_{ij}) and the heat flux vector (q_i) in $\tilde{f}_2$ presented in Eq. (9). The quantities σ_{ij} and q_i are obtained as the higher-order moments of f, which, at the N–S level of approximation, are given as

$$\begin{aligned} \sigma^{NS}_{ij} = \langle C_{\langle i} C_{j \rangle}, \tilde{f}_1 \rangle = -2\mu \left(\frac{1}{2} \left[\frac{\partial u_i}{\partial x_j} + \frac{\partial u_j}{\partial x_i} \right] - \frac{1}{3} \frac{\partial u_l}{\partial x_l} \delta_{ij} \right) = -2\mu \frac{\partial u_{\langle i}}{\partial x_{j \rangle}}, \\ q^{NS}_i = \frac{1}{2} \langle |\boldsymbol{C}|^2 C_i, \tilde{f}_1 \rangle = -\kappa \frac{\partial T}{\partial x_i}, \end{aligned} \tag{22}$$

where angular bracket ($\langle\rangle$) used in subscript in tensor notation denotes trace-free symmetric tensor. Note that the higher-order moments of the Maxwellian identically vanish to yield the inviscid and isentropic behavior of the Euler equations.

The use of the N–S equations in Eq. (11) amounts to relaxing the inviscid and isentropic assumptions inherent to the Euler equations, thus resulting in an $\mathcal{O}(\mathrm{Kn}^3)$ representation of f_2; this third-order representation can be given as

$$f_2^{\mathcal{O}(\mathrm{Kn}^3)} = f_2^{\mathcal{O}(\mathrm{Kn}^2)} + \underbrace{(\boldsymbol{\Upsilon}''_{\tau\tau} \odot \boldsymbol{X}_\tau) \odot \boldsymbol{X}_\tau + (\boldsymbol{\Upsilon}''_{qq} \odot \boldsymbol{X}_q) \odot \boldsymbol{X}_q}_{\tilde{f}_3}, \tag{23}$$

where the double prime superscript is used to denote the $\mathcal{O}(\mathrm{Kn}^3)$ correction to the microscopic flux tensor $\boldsymbol{\Upsilon}_i$. Explicitly, we obtain the correction terms of Eq. (23) as

$$\begin{aligned} (\boldsymbol{\Upsilon}''_{\tau\tau} \odot \boldsymbol{X}_\tau) = t^2_{r(\tau)} f_0 \left\{ -\tilde{\boldsymbol{\Upsilon}}_\tau \left[\frac{4\beta^2}{3\rho} \Omega \left(\frac{3}{2\beta} - C_l^2 \right) - \frac{2\beta C_l}{\rho} \frac{\partial \sigma^{NS}_{lk}}{\partial x_k} \right] \right. \\ + \tilde{\boldsymbol{\Upsilon}}_\tau \left[(\varphi - 1) \frac{4\beta}{3\rho} \Omega \right] + \left[\frac{1}{\rho} \frac{\partial \sigma^{NS}_{ik}}{\partial x_k} C_j + \frac{1}{\rho} C_i \frac{\partial \sigma^{NS}_{jk}}{\partial x_k} \right. \\ \left. \left. - \frac{2}{3} C_k \frac{1}{\rho} \frac{\partial \sigma^{NS}_{kl}}{\partial x_l} \delta_{ij} \right] \right\}, \end{aligned} \tag{24}$$

and

$$\begin{aligned} (\boldsymbol{\Upsilon}''_{qq} \odot \boldsymbol{X}_q) = \; t^2_{r(q)} f_0 \left\{ -\tilde{\boldsymbol{\Upsilon}}_q \left[\frac{4\beta^2}{3\rho} \Omega \left(\frac{3}{2\beta} - C_l^2 \right) - \frac{2\beta C_l}{\rho} \frac{\partial \sigma^{NS}_{lk}}{\partial x_k} \right] \right. \\ + \tilde{\boldsymbol{\Upsilon}}_q \left[(\varphi - 1) \frac{4\beta}{3\rho} \Omega \right] + \left[C_i \left(-\frac{10}{3\rho} \Omega - \frac{2}{\rho} C_k \frac{\partial \sigma^{NS}_{kj}}{\partial x_j} \right) \right. \\ \left. \left. + \left(\frac{5}{2\beta} - |C|^2 \right) \left(\frac{1}{\rho} \frac{\partial \sigma^{NS}_{ij}}{\partial x_j} \right) \right] \right\}, \end{aligned} \tag{25}$$

where Ω is defined as

$$\Omega = \left[\frac{\partial q^{NS}_l}{\partial x_l} + \sigma^{NS}_{lk} \frac{\partial u_l}{\partial x_k} \right]. \tag{26}$$

We next check for the additive invariance condition and find that, since $\langle \Psi, \tilde{f}_3 \rangle$ is identically zero, Eq. (23) does not require any modifications.

III. GENERALIZED SET OF 13-MOMENT EQUATIONS

The generalized, three-dimensional 13-moment equations are obtained by evaluating moments of the Boltzmann Equation given in Eq. (1). Explicitly, this evaluation, which amounts to computing $\left\langle \Psi, \frac{\partial f}{\partial t} + \frac{\partial}{\partial \boldsymbol{x}} \cdot (\boldsymbol{c} f) \right\rangle = \langle \Psi, \mathscr{J}(f,f) \rangle$, where $\Psi = \left\{ 1, c_i, \frac{C_i^2}{2}, C_{\langle i} C_{j \rangle}, C_i \frac{C_k^2}{2} \right\}$, yields[10,13]

$$\frac{\partial \rho}{\partial t} + \frac{\partial \rho u_k}{\partial x_k} = 0, \tag{27}$$

$$\rho \frac{\partial u_i}{\partial t} + \rho u_k \frac{\partial u_i}{\partial x_k} + \frac{\partial p}{\partial x_i} + \frac{\partial \sigma_{ik}}{\partial x_k} = 0, \tag{28}$$

$$\rho \frac{\partial \varepsilon}{\partial t} + \rho u_k \frac{\partial \varepsilon}{\partial x_k} + \frac{\partial q_k}{\partial x_k} + p \frac{\partial u_k}{\partial x_k} + \sigma_{ij} \frac{\partial u_i}{\partial x_j} = 0, \tag{29}$$

$$\frac{\partial \sigma_{ij}}{\partial t} + u_k \frac{\partial \sigma_{ij}}{\partial x_k} + \frac{4}{5} \frac{q_{\langle i}}{\partial x_{j \rangle}} + 2\sigma_{k\langle i} \frac{\partial u_{j\rangle}}{\partial x_k} + 2p \frac{\partial u_{\langle i}}{\partial x_{j\rangle}} + \sigma_{ij} \frac{\partial u_k}{\partial x_k} + \frac{\partial}{\partial x_k} \langle C_{<i} C_j C_{k>}, f \rangle = \langle C_{\langle i} C_{j \rangle}, \mathscr{J}(f,f) \rangle, \tag{30}$$

$$\frac{\partial q_i}{\partial t} + u_k \frac{\partial q_i}{\partial x_k} + \frac{5}{2} \left(\frac{p}{\rho} \frac{\partial p}{\partial x_i} - \frac{p^2}{\rho^2} \frac{\partial \rho}{\partial x_i} \right) + \frac{\partial}{\partial x_k} \frac{1}{2} \langle |C|^2 C_{<i} C_{j>}, f \rangle - \frac{5}{2} \frac{p}{\rho} \frac{\partial \sigma_{ik}}{\partial x_k} - \frac{\sigma_{ik}}{\rho} \frac{\partial p}{\partial x_k} + \frac{1}{6} \frac{\partial}{\partial x_i} \langle |C|^4, (f - f_0) \rangle - \frac{\sigma_{ij}}{\rho} \frac{\partial \sigma_{ij}}{\partial x_k} + \frac{7}{5} q_k \frac{\partial u_i}{\partial x_k} + \frac{7}{5} q_i \frac{\partial u_k}{\partial x_k} + \frac{2}{5} q_k \frac{\partial u_k}{\partial x_i} + \frac{\partial u_j}{\partial x_k} \langle C_{<i} C_j C_{k>}, f \rangle = \frac{1}{2} \langle |\boldsymbol{C}|^2 C_i, \mathscr{J}(f,f) \rangle, \tag{31}$$

where $\varepsilon = (3/2)RT$ is the internal energy, while $p = \rho RT$ is the thermodynamic pressure as represented by the ideal gas law. Equations (27)–(29) are the three famous hydrodynamic conservation equations. Note that the production terms in these equations, $\left\langle \left\{ 1, c_i, \frac{C_i^2}{2} \right\}, \mathscr{J}(f,f) \right\rangle$, vanish following the principles of conservation of mass, momentum, and energy for particles undergoing elastic collisions. For Eqs. (30) and (31), which describe the evolution of the stress tensor and heat flux vector, the production terms appear on the right-hand side. For Maxwell molecules, these production terms obtained by using the BGK collision model have been given as[50]

$$\langle C_{\langle i} C_{j \rangle}, \mathscr{J}(f,f) \rangle = -\frac{p}{\mu} \sigma_{ij}, \tag{32}$$

$$\frac{1}{2} \left\langle |\boldsymbol{C}|^2 C_i, \mathscr{J}(f,f) \right\rangle = -\frac{2}{3} \frac{p}{\mu} q_i, \tag{33}$$

where σ_{ij} and q_i contain first- and second-order contributions. Equations (30) and (31) contain three unknown higher-order moments, which need to be computed for closure.

Third-order accurate representations of the moments $\langle C_{\langle i} C_j C_{k \rangle}, f \rangle$ and $\langle C_i^4, (f - f_0) \rangle$ are evaluated by using Eq. (23) as

$$\left\langle C_{\langle i} C_j C_{k \rangle}, f_2^{\mathscr{O}(\mathrm{Kn}^3)} \right\rangle = \left\langle C_{\langle i} C_j C_{k \rangle}, f_2^{\mathscr{O}(\mathrm{Kn}^2)} \right\rangle - \frac{3}{\beta} t_{r_\tau}^2 \frac{\partial \sigma_{<il}^{NS}}{\partial x_l} \frac{\partial u_j}{\partial x_{k>}}, \tag{34}$$

$$\left\langle |\boldsymbol{C}|^4, \left(f_2^{\mathscr{O}(\mathrm{Kn}^3)} - f_0 \right) \right\rangle = \left\langle |\boldsymbol{C}|^4, \left(f_2^{\mathscr{O}(\mathrm{Kn}^2)} - f_0 \right) \right\rangle + t_{r_q}^2 \frac{5}{\beta^3} \left(\frac{\partial \sigma_{ij}^{NS}}{\partial x_j} \frac{\beta q_i^{NS}}{\kappa T} \right), \tag{35}$$

with the corresponding second-order accurate moments, evaluated using Eq. (19), being given as

$$\left\langle C_{\langle i} C_j C_{k \rangle}, f_2^{\mathscr{O}(\mathrm{Kn}^2)} \right\rangle = \frac{3\rho}{2\beta^3} \left(\left[-t_{r_q}^2 \frac{\beta q_{<i}^{NS}}{\kappa T} \frac{\partial u_j}{\partial x_{k>}} - t_{r_\tau}^2 \frac{\beta q_{<i}^{NS}}{\kappa T} \frac{\partial u_j}{\partial x_{k>}} \right] - \beta t_{r_\tau}^2 \frac{\partial g}{\partial x_{<i}} \frac{\partial u_j}{\partial x_{k>}} \right), \tag{36}$$

and

$$\left\langle |\boldsymbol{C}|^4, \left(f_2^{\mathscr{O}(\mathrm{Kn}^2)} - f_0 \right) \right\rangle = t_{r_q}^2 \frac{5\rho}{2\beta^5} \left(\frac{7}{2} \frac{\beta q_l^{NS}}{\kappa T} \frac{\beta q_l^{NS}}{\kappa T} + \beta \frac{\partial g}{\partial x_l} \frac{\beta q_l^{NS}}{\kappa T} \right). \tag{37}$$

An explicit evaluation using Eq. (19) yields

$$\left\langle \frac{1}{2} C_k^2 C_{<i} C_{j>}, f_2^{\mathscr{O}(\mathrm{Kn}^2)} \right\rangle = \frac{7}{4\beta} \left[\sigma_{ij} + \frac{(2\varphi - 5)}{6\mu} \frac{\rho t_{r_\tau}^2}{\beta} \frac{\partial u_l}{\partial x_l} \sigma_{ij}^{NS} + \frac{\rho}{2\beta^4} t_{r_q}^2 \times \left(2 \frac{\beta q_{<i}^{NS}}{\kappa T} \frac{\beta q_{i>}^{NS}}{\kappa T} + \beta \frac{\beta q_{<i}^{NS}}{\kappa T} \frac{\partial g}{\partial x_{j>}} \right) \right], \tag{38}$$

and a similar evaluation using Eq. (23) yields

$$\left\langle \frac{1}{2} C_k^2 C_{<i} C_{j>}, f_2^{\mathscr{O}(\mathrm{Kn}^3)} \right\rangle = \left\langle \frac{1}{2} C_k^2 C_{<i} C_{j>}, f_2^{\mathscr{O}(\mathrm{Kn}^2)} \right\rangle + \frac{7}{4\beta} \times \left(-\frac{4(\varphi + 2)}{3} t_{r_\tau}^2 \frac{\partial u_{<i}}{\partial x_{j>}} \left(\frac{\partial q_l^{NS}}{\partial x_l} + \sigma_{lk}^{NS} \frac{\partial u_l}{\partial x_k} \right) + t_{r_q}^2 \frac{1}{\beta^2} \frac{\partial \sigma_{<il}^{NS}}{\partial x_l} \frac{\beta q_{j>}^{NS}}{\kappa T} \right), \tag{39}$$

where $\bar{\sigma}_{ij}^{\mathscr{O}(\mathrm{Kn}^3)}$ is a third-order correction to the second-order accurate constitutive relationship for the stress tensor of second order $\left(\sigma_{ij}^{\mathscr{O}(\mathrm{Kn}^2)} \right)$.

To summarize, the proposed set of 13-moment equations is presented by Eqs. (27)–(31) and form a second-order- and third-order accurate representation of hydrodynamics upon using expressions presented in Eqs. (32)–(39).

IV. MODIFIED GOVERNING EQUATIONS

The governing equations presented in Sec. III lack linear terms that are necessary for capturing the near-wall Knudsen layer effects.[32] Thus, following Timokhin *et al.*,[51] we first modify the proposed governing equations by expressing them in an alternate form, then we replace the Navier–Stokes stress tensor and heat flux (σ_{ij}^{NS}, q_i^{NS}) with the full stress tensor and heat flux vector (σ_{ij}, q_i) in the closure relations presented in Eqs. (34)–(39), followed by incorporating primary variables. Note that only the N–S stress tensor has been used to write Eqs. (34)–(39) into an alternate form as presented by Eqs. (40)–(45). Explicitly, the proposed alternate form of closure relations Eqs. (34)–(39) is given as

$$\left\langle C_{\langle i}C_jC_{k\rangle}, f_2^{\mathcal{O}(\mathrm{Kn}^3)}\right\rangle = \left\langle C_{\langle i}C_jC_{k\rangle}, f_2^{\mathcal{O}(\mathrm{Kn}^2)}\right\rangle - \frac{3}{\beta}t_{r_\tau}^2\frac{\partial\sigma_{<il}}{\partial x_l}\frac{\partial u_j}{\partial x_{k>}}, \quad (40)$$

$$\left\langle C_i^4, \left(f_2^{\mathcal{O}(\mathrm{Kn}^3)} - f_0\right)\right\rangle = \left\langle C_i^4, \left(f_2^{\mathcal{O}(\mathrm{Kn}^2)} - f_0\right)\right\rangle + t_{r_q}^2\frac{5}{\beta^3}\left(\frac{\partial\sigma_{ij}}{\partial x_j}\frac{\beta q_i}{\kappa T}\right), \quad (41)$$

$$\left\langle C_{\langle i}C_jC_{k\rangle}, f_2^{\mathcal{O}(\mathrm{Kn}^2)}\right\rangle = \frac{3\rho}{2\beta^3}\left(\left[-t_{r_q}^2\frac{\beta q_{<i}}{\kappa T}\frac{\partial u_j}{\partial x_{k>}} - t_{r_\tau}^2\frac{\beta q_{<i}}{\kappa T}\frac{\partial u_j}{\partial x_{k>}}\right] - \beta t_{r_\tau}^2\frac{\partial g}{\partial x_{<i}}\frac{\partial u_j}{\partial x_{k>}}\right), \quad (42)$$

$$\left\langle C_i^4, \left(f_2^{\mathcal{O}(\mathrm{Kn}^2)} - f_0\right)\right\rangle = t_{r_q}^2\frac{5\rho}{2\beta^5}\left(\frac{7}{2}\frac{\beta q_l}{\kappa T}\frac{\beta q_l}{\kappa T} + \beta\frac{\partial g}{\partial x_l}\frac{\beta q_l}{\kappa T}\right), \quad (43)$$

$$\left\langle \frac{1}{2}C_k^2C_{<i}C_{j>}, f_2^{\mathcal{O}(\mathrm{Kn}^2)}\right\rangle = \frac{7}{4\beta}\left[2\sigma_{ij} + \frac{(2\varphi-5)}{6\mu}\frac{\rho t_{r_\tau}^2}{\beta}\frac{\partial u_l}{\partial x_l}\sigma_{ij} + 2t_{r_\tau}\left(\frac{p}{2}\left[\frac{\partial u_i}{\partial x_j} + \frac{\partial u_j}{\partial x_i}\right]\right) - 2t_{r_\tau}\left(\frac{p}{3}\frac{\partial u_l}{\partial x_l}\delta_{ij}\right) + \frac{\rho}{2\beta^4}t_{r_q}^2\left(2\frac{\beta q_{<i}}{\kappa T}\frac{\beta q_{i>}}{\kappa T} + \beta\frac{\beta q_{<i}}{\kappa T}\frac{\partial g}{\partial x_{j>}}\right)\right], \quad (44)$$

and

$$\left\langle \frac{1}{2}C_k^2C_{<i}C_{j>}, f_2^{\mathcal{O}(\mathrm{Kn}^3)}\right\rangle = \left\langle \frac{1}{2}C_k^2C_{<i}C_{j>}, f_2^{\mathcal{O}(\mathrm{Kn}^2)}\right\rangle + \frac{7}{4\beta} \times \left(-\frac{4(\varphi+2)}{3}t_{r_\tau}^2\frac{\partial u_{<i}}{\partial x_{j>}}\left(\frac{\partial q_l}{\partial x_l} + \sigma_{lk}\frac{\partial u_l}{\partial x_k}\right) + t_{r_q}^2\frac{1}{\beta^2}\frac{\partial\sigma_{<il}}{\partial x_l}\frac{\beta q_{j>}}{\kappa T}\right). \quad (45)$$

V. VALIDATION

A. Grad's second problem

We investigate the behavior of the proposed set of modified moment equations (including the third-order accurate terms) for Grad's second problem (see Fig. 1), wherein the steady state solution of the temperature field of an enclosed quiescent gas under the influence of an externally supplied heat flux is evaluated. Note that the non-zero Knudsen number establishes a temperature jump at the walls,[10] which necessitates the use of Knudsen number-dependent boundary conditions to account for wall effects. However, since Grad's second flow problem considers the flow domain to be beyond the influence of the Knudsen layers,[13] it does not involve any physical boundaries, thereby circumventing the need for deriving wall boundaries conditions needed for evaluating the accuracy of higher-order transport equations for canonical boundary value problems. To obtain the solution for the considered problem, we first simplify Eqs. (27)–(31) by applying the steady state and quiescent flow conditions. We find that Eq. (27) identically vanishes, while Eqs. (28)–(30) yield

$$\frac{dp}{dx} = 0, \quad (46a)$$

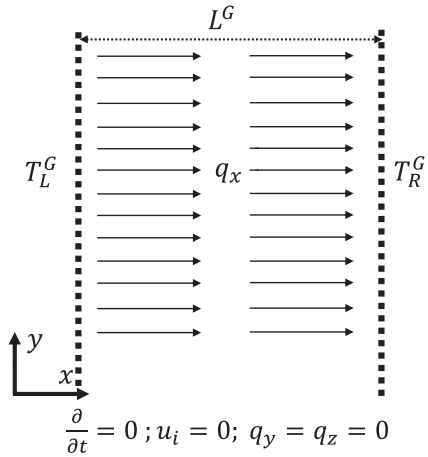

FIG. 1. For Grad's second problem, the imaginary boundary is assumed to be away from the physical wall to avoid the complexity due to the temperature jump. The physical and imaginary walls are separated by a distance of L and $L^G < L$, respectively. The two walls are subjected to a constant heat flux q_x and are subjected to boundary temperatures of T_L and T_R at the left and right walls, respectively, when thermal jumps are not included.

$$\frac{dq_x}{dx} = 0, \quad (46b)$$

$$\sigma_{ij} = 0. \quad (46c)$$

Here, it is noteworthy that the pressure field and heat flux are obtained as constant functions, while the stress tensor vanishes throughout the flow domain. Thereafter, using Eq. (46) in conjunction with the ideal gas law, Eq. (31) is further simplified to obtain the spatial evolution of the temperature field as

$$q_x = -\kappa\frac{dT}{d\mathbf{x}}, \quad (47)$$

where the thermal conductivity and dynamic viscosity are related as $\kappa = \frac{15}{4}R\mu$. For the Maxwell molecules, substituting $\kappa = B_1T$,[52] where $B_1 = \kappa_o/T_o$ is a proportional constant, in Eq. (47) provides

$$T\frac{dT}{d\mathbf{x}} = -\frac{q_x}{B_1} = \text{constant}. \quad (48)$$

We analytically solve the boundary value problem presented by the first-order, non-linear, ordinary differential equation presented in Eq. (48) as

$$T = \sqrt{\frac{2(-q_xx + B_1C_1)}{B_1}}, \quad (49)$$

where C_1 is an integration constant. Note that the solution of G13 equations also provides the same result as presented in Ref. 53. The required parameters to obtain C_1 are taken from the work by Gallis, Torczynski, and Rader[54] who address Fourier's problem for Maxwell's molecules by using the direct simulation Monte Carlo method (DSMC). The Knudsen number was taken to be Kn = 0.0237 with the reference values being $p_0 = 266.6$ Pa, $\mu_0 = 2.117 \times 10^{-5}$ Pa s, $\kappa_0 = 2.247$ W/mK, and $T_0 = 273.15$ K.

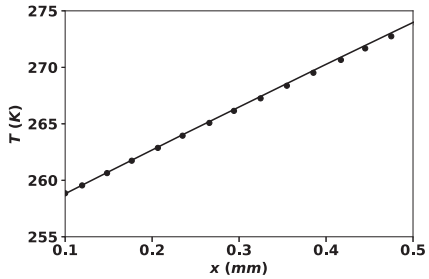

FIG. 2. Comparison of temperature profile for Maxwell molecules and DSMC results[54] for Grad's second problem at Kn = 0.0232. The continuous line represents the results given by Eq. (49), while the solid circles represent the DSMC results.

The heat flux was $q_x = -\kappa_0 \frac{(T_H - T_C)}{L}$ W/m^2, where $T_H, T_C = T_0 \pm 20$ K and $L = 1 \times 10^{-3}$ m. The analytical results are presented in Fig. 2 only for $0.1 \le x \le 0.5$, where $T_L^G = 258.7914$ K. The solution of Eq. (49) agrees well with the DSMC result, where the effect of temperature jumps has been excluded by considering the flow domain some mean free path length away from the wall as followed in Refs. 52, 53, 55, and 56.

B. Force-driven compressible plane Poiseuille problem

In this section, we validate the proposed set of modified equations for the well-known two-dimensional force-driven compressible plane Poiseuille flow problem. To simplify the analysis, we assume the flow to be steady and that all primary variables are functions of spanwise direction only. Note that the normal velocity (v) component is zero due to the impermeable bounding walls.

The above conditions result in the following simplifications:

$$\begin{aligned} u_i &= \{u_1(y), 0, 0\}, \\ \sigma_{ij} &= \{\sigma_{11}(y), \sigma_{12}(y), \sigma_{21}(y), \sigma_{22}(y), -\sigma_{11}(y) - \sigma_{22}(y)\}, \\ q_i &= \{q_1(y), q_2(y)\}. \end{aligned} \tag{50}$$

As shown in Fig. 3, both parallel plates are separated by distance H, and the origin is located at the center and the entrance of the channel. The viscosity (μ) is assumed to be independent of temperature leading to isothermal flow conditions. Introducing the following non-dimensional variables,

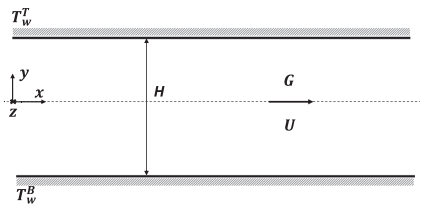

FIG. 3. Schematic of compressible plane Poiseuille flow problem driven by an external force (G), where U represent the flow direction, and T_w^T and T_w^B are the temperature of upper and lower plates, respectively.

$$\begin{aligned} \tilde{y} = \frac{y}{H}, \tilde{\rho} = \frac{\rho - \rho_o}{\rho_o}, \tilde{T} = \frac{T - T_o}{T_o}, \tilde{G} = \frac{H}{RT_o} G, \tilde{u}_1 = \frac{u_1}{\sqrt{RT_o}}, \\ \tilde{\sigma}_{ij} = \frac{\sigma_{ij}}{\rho_o \sqrt{RT_o}}, \tilde{q}_1 = \frac{q_1}{\rho_o \sqrt{RT_o{}^3}}, \end{aligned} \tag{51}$$

into Eqs. (27)–(31) yields

$$x\text{–Momentum equation} : -\tilde{G} + \frac{d\tilde{\sigma}_{12}}{d\tilde{y}} = 0, \tag{52a}$$

$$y\text{–Momentum equation} : \frac{d\tilde{T}}{d\tilde{y}} + \frac{d\tilde{\rho}}{d\tilde{y}} + \frac{d\tilde{\sigma}_{22}}{d\tilde{y}} = 0, \tag{52b}$$

$$\text{Energy equation} : \tilde{\sigma}_{12} \frac{d}{d\tilde{y}} \tilde{u}_1 + \frac{d}{d\tilde{y}} \tilde{q}_2 = 0, \tag{53}$$

$$\tilde{\sigma}_{11} \quad \text{Stress equation} : \frac{4}{3} \tilde{\sigma}_{12} \frac{d\tilde{u}_1}{d\tilde{y}} - \frac{4}{15} \frac{d\tilde{q}_2}{d\tilde{y}} + \frac{\tilde{\sigma}_{11}}{Kn} = 0, \tag{54a}$$

$$\tilde{\sigma}_{12} \quad \text{Stress equation} : \frac{2}{5} \frac{d\tilde{q}_1}{d\tilde{y}} + \frac{d\tilde{u}_1}{d\tilde{y}} + \frac{\tilde{\sigma}_{12}}{Kn} = 0, \tag{54b}$$

$$\tilde{\sigma}_{22} \quad \text{Stress equation} : -\frac{2}{3} \tilde{\sigma}_{12} \frac{d\tilde{u}_1}{d\tilde{y}} + \frac{8}{15} \frac{d\tilde{q}_2}{d\tilde{y}} + \frac{\tilde{\sigma}_{22}}{Kn} = 0, \tag{54c}$$

$$\tilde{q}_1 \quad \text{Heat equation} : \frac{7}{4} Kn \frac{d^2 \tilde{u}_1}{d\tilde{y}^2} + \frac{9}{4} \frac{d\tilde{\sigma}_{12}}{d\tilde{y}} + \frac{\tilde{q}_1}{3Kn} = 0, \tag{55a}$$

$$\tilde{q}_2 \quad \text{Heat equation} : \frac{2}{5} \tilde{q}_1 \frac{d\tilde{u}_1}{d\tilde{y}} + \frac{5}{2} \frac{d\tilde{T}}{d\tilde{y}} + \frac{9}{2} \frac{d\tilde{\sigma}_{22}}{d\tilde{y}} + \frac{2\tilde{q}_2}{3Kn} = 0. \tag{55b}$$

Note that the Knudsen number ($Kn = \mu_0 \sqrt{RT_0}/p_0 H$) and non-dimensional variables are defined by using the equilibrium state $\{\rho_0, T_0, u_0 = 0\}$. Furthermore, note that in Eqs. (52a)–(55b), we retain some important non-linear terms, such as $\tilde{\sigma}_{21} \frac{d\tilde{u}_1}{d\tilde{y}}$, $\tilde{q}_1 \frac{d\tilde{u}_1}{d\tilde{y}}$, and $\tilde{q}_2 \frac{d\tilde{u}_1}{d\tilde{y}}$ in addition to all the linear terms to accounts for viscous heating and non-hydrodynamic effects such as the presence of the Knudsen boundary layer that is observed in the present problem.[32]

By integrating Eq. (52a), we obtain

$$\tilde{\sigma}_{21} = \underline{\tilde{G}\tilde{y}} + \underline{C_{\sigma_{21}}}, \tag{56}$$

where $C_{\sigma_{21}}$ is an integration constant. The underlined terms here, and in the following sentences, reflect the solution when the G13 equations are applied to the present problem. Thereafter, simultaneously solving the coupled Eqs. (55a) and (54b) after incorporating Eq. (56) gives us

$$\tilde{q}_1 = C_{q11} \sinh\left(\frac{\sqrt{210}\tilde{y}}{21Kn}\right) + C_{q12} \cosh\left(\frac{\sqrt{210}\tilde{y}}{21Kn}\right) - \underline{\frac{3\tilde{G}Kn}{2}}, \tag{57}$$

$$\tilde{u}_1 = -\frac{2C_{q11} \sinh\left(\frac{\sqrt{210}\tilde{y}}{21Kn}\right)}{5} - \frac{2C_{q12} \cosh\left(\frac{\sqrt{210}\tilde{y}}{21Kn}\right)}{5} + \underline{C_{u1}} - \underline{\frac{\tilde{G}\tilde{y}^2}{2Kn}} - \underline{C_{\sigma_{21}}\tilde{y}}, \tag{58}$$

where C_{q11}, C_{q12}, and C_{u1} are the integration constants. It is important to mention that the N–S equations yield zero stream-wise heat

flux, while the G13 equations provide a constant heat flux. Finally, after incorporating Eqs. (56)–(58) into Eq. (53), we can obtain

$$\begin{aligned}\bar{q}_2 = C_{q11}&\left(-\frac{\sqrt{210}\bar{G}Kn\,\cosh\left(\frac{\sqrt{210}\bar{y}}{21Kn}\right)}{25}+\frac{2\bar{G}\bar{y}\sinh\left(\frac{\sqrt{210}\bar{y}}{21Kn}\right)}{5}\right)\\&+C_{q12}\left(-\frac{\sqrt{210}\bar{G}Kn\,\sinh\left(\frac{\sqrt{210}\bar{y}}{21Kn}\right)}{25}+\frac{2\bar{G}\bar{y}\cosh\left(\frac{\sqrt{210}\bar{y}}{21Kn}\right)}{5}\right)\\&+C_{\sigma21}\left(\frac{2C_{q11}\,\sinh\left(\frac{\sqrt{210}\bar{y}}{21Kn}\right)}{5}+\frac{2C_{q12}\,\cosh\left(\frac{\sqrt{210}\bar{y}}{21Kn}\right)}{5}+\frac{\bar{G}\bar{y}^2}{Kn}\right)\\&+\underline{C_{q23}}+\underline{\frac{C_{\sigma21}^2\bar{y}}{Kn}}+\underline{\frac{\bar{G}^2\bar{y}^3}{3Kn}},\end{aligned}\tag{59}$$

where we note that the constants of integration, $C_{\sigma21}$, C_{q11}, and C_{q23}, appearing in Eqs. (56)–(59) vanish upon incorporating the symmetry demonstrated by the stream-wise velocity and heat flux.

In Figs. 4–7, the analytical solutions presented in Eqs. (56)–(59) are compared with DSMC results used by Taheri, Torrilhon, and Struchtrup[32] and the solutions obtained by using the G13 equations for a non-dimensional force $\bar{G} = 0.2355$ and Knudsen number $Kn = 0.072$. Note that it has been previously established that the G13 equations are unable to capture the Knudsen layer effects of wall-bounded flows. Following Rath, Yadav, and Agrawal[57] and Rath, Singh, and Agrawal,[58] remaining integration constants, C_{q12} and C_{u1}, have been computed from the existing DSMC data. Figure 4 shows the variation of shear stress tensor ($\bar{\sigma}_{21}$), which is linear and transitions from negative to positive values at the center of the channel. It can be seen that the profiles of the shear stress tensor obtained from the present and G13 equations are indistinguishable. In Fig. 5, the stream-wise heat flux ($\bar{q}_1$) agrees with DSMC results in the near-wall regions and yields a fairly good agreement in the regions away from the wall. In contrast, the solution derived from the G13 equations remains constant throughout the flow domain. The stream-wise velocity ($\bar{u}_1$) profile, shown in Fig. 6, is largest at the center and yields better agreement with DSMC results as compared to G13 equations in the bulk of the fluid. Finally, similar to Fig. 4, Fig. 7 shows that the cross stream-wise heat flux ($\bar{q}_2$) obtained with the proposed equations agrees well with the DSMC results and is indistinguishable from the G13 results only away from the boundaries. However, close observation reveals that the proposed equations perform better than the G13 equations near the boundaries due to the presence of additional hyperbolic terms that are responsible for capturing the Knudsen layer. This difference between the present and G13 equations becomes more observable at higher Knudsen numbers.

In summary, we find an excellent qualitative and quantitative agreement between the analytical solution of the proposed equations and DSMC results for $\bar{\sigma}_{21}$, $\bar{u}_1$, and $\bar{q}_2$. However, some quantitative discrepancy between $\bar{q}_1$ and DSMC results can be observed, which might be due to the isothermal assumption used in this paper. On the other hand, the solution of G13 equations fails to provide the same consistency against the DSMC results.

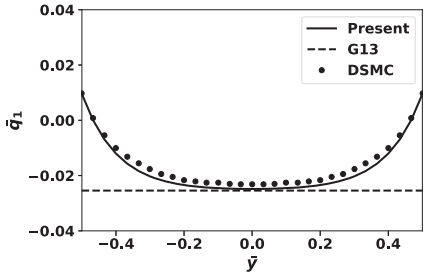

FIG. 5. Comparison of $\bar{q}_1$ profile against DSMC results used by Taheri, Torrilhon, and Struchtrup[32] for $Kn = 0.072$ and $\bar{G} = 0.2355$.

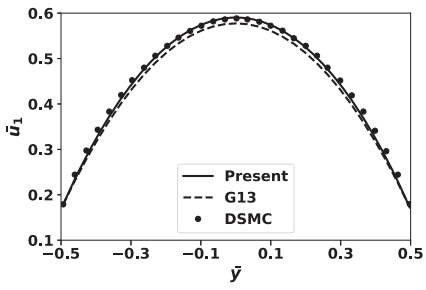

FIG. 6. Comparison of $\bar{u}_1$ profile against DSMC results used by Taheri, Torrilhon, and Struchtrup[32] for $Kn = 0.072$ and $\bar{G} = 0.2355$.

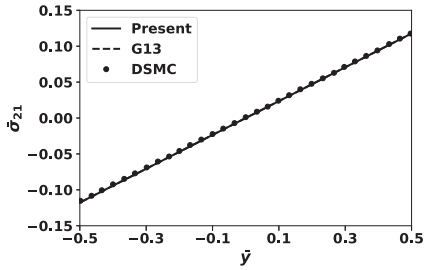

FIG. 4. Comparison of $\bar{\sigma}_{21}$ profile against DSMC results used by Taheri, Torrilhon, and Struchtrup[32] for $Kn = 0.072$ and $\bar{G} = 0.2355$.

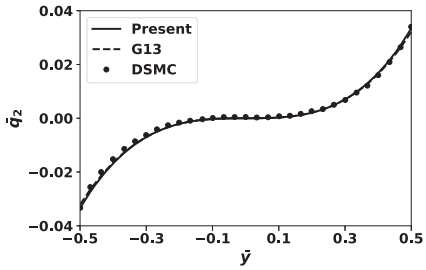

FIG. 7. Comparison of $\bar{q}_2$ profile against DSMC results used by Taheri, Torrilhon, and Struchtrup[32] for $Kn = 0.072$ and $\bar{G} = 0.2355$.

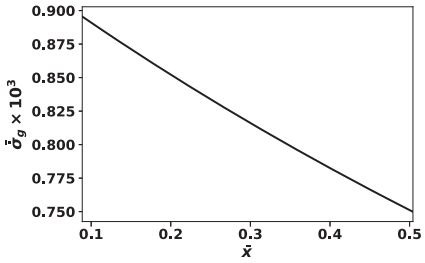

FIG. 8. Non-dimensional entropy production rate ($\bar{\dot{\sigma}}_g$) for Grad's second problem.

C. Entropy analysis

In this section, we perform an entropy analysis to demonstrate compliance of the proposed equations with the second law of thermodynamics for the two validation problems considered in this paper. Here, we use the entropy balance equation that is obtained from a continuum viewpoint,[59]

$$\rho \frac{Ds_{eq}}{Dt} + \nabla \cdot \mathbf{J} = \dot{\sigma}_g, \tag{60}$$

where s_{eq} is the specific entropy, $\mathbf{J} = \mathbf{q}/T$ represents the entropy flux, and the classical entropy generation term, $\dot{\sigma}_g$, is given as[60,61]

$$\dot{\sigma}_g = \frac{\tau_{ij}}{T}\frac{\partial u_i}{\partial x_j} - \frac{q_j}{T^2}\frac{\partial T}{\partial x_j}. \tag{61}$$

Equation (61) represents the rate of irreversible entropy production, which must be positive and definite per the second law of thermodynamics. Here, τ_{ij} represents the viscous stress tensor and is related to the pressure tensor through the relation $\sigma_{ij} = -\tau_{ij}$.[10]

In the case of Grad's second problem, only thermal diffusion contributes to the entropy generation in Eq. (61) since the stress tensor (σ_{ij}) vanishes, as shown in Eq. (46). In contrast, for the plane Poiseuille flow problem, only viscous dissipation contributes to the entropy generation due to the isothermal assumption. In Figs. 8 and 9, we present the variation of the non-dimensional entropy generation, $\bar{\dot{\sigma}}_g$. For Grad's second problem, Fig. 8 shows that $\bar{\dot{\sigma}}_g$ is largest and least near the left and right boundaries corresponding to the largest and least temperature gradient. Furthermore, $\bar{\dot{\sigma}}_g$ monotonically decreases from the left to right boundary. Similarly, as shown in Fig. 9, for the plane Poiseuille flow problem, $\bar{\dot{\sigma}}_g$ monotonically decreases from a maximum value at the walls of the channel and vanishes at the center. Thus, the second law of thermodynamics holds for the solutions obtained with the proposed equations for both considered problems.

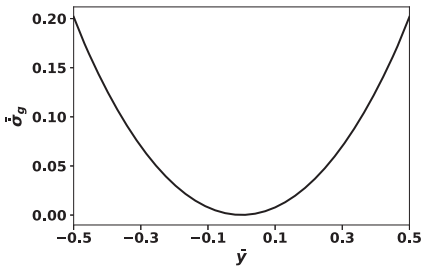

FIG. 9. Non-dimensional entropy production rate ($\bar{\dot{\sigma}}_g$) for force-driven Poiseuille flow problem.

VI. DISCUSSION

The system of equations presented by Eqs. (15) and (16) is under-determined and can admit several solutions. Thus, one can construct multiple representations of the second-order approximation of the distribution function, f_2. In this paper, we present a compact representation of f_2 that is easier to manage due to the presence of fewer terms as compared to that proposed previously by Singh and Agrawal.[36] Moreover, since both the earlier and current $\mathcal{O}(\mathrm{Kn}^2)$ forms of f_2 are obtained from identical derivation procedures, the second-order accurate macroscopic governing equations obtained from Eqs. (19)–(21) are expected to retain the overall characteristic features of those proposed earlier. Furthermore, the $\mathcal{O}(\mathrm{Kn}^2)$ accurate 13-moment equations derived by using the $\mathcal{O}(\mathrm{Kn}^2)$ form of f_2 are found to not only have more terms in comparison to the G13 equations but also have fewer terms when compared to the moment equations presented by Singh and Agrawal;[36] the latter is a direct consequence of f_2 having a more compact form. These additional terms appear from the closure relations $m\langle C_{\langle i}C_jC_{k\rangle}, f_2\rangle$ and $m\langle C_i^4, (f_2 - f_0)\rangle$ as evaluated in Eqs. (34) and (35). In stark contrast, these two moments are identically zero in the case of G13 equations.[10,36]

However, it is noteworthy that the Euler equations employed in deriving the $\mathcal{O}(\mathrm{Kn}^2)$ forms of f_2 incorporate inviscid and isentropic assumptions that have been previously shown to limit the applicability of second-order accurate macroscopic governing equations to small departures from the equilibrium state.[49,62] Thus, this paper also presents a first-principles-based derivation of $\mathcal{O}(\mathrm{Kn}^3)$ corrections to obtain third-order accurate representations of f_2. These corrections satisfy the additive invariance property as-is and are therefore unique. As is expected, the third-order accurate 13-moment representation derived by using the $\mathcal{O}(\mathrm{Kn}^3)$ form of f_2 has even more terms as compared to G13 and the proposed second-order accurate 13-moment representation. However, as is easily verifiable upon non-dimensionalization, it is important to note that the closure relations for the proposed equations contain nonlinear terms from both the Burnett and super-Burnett levels. In contrast, the $\mathcal{O}(\mathrm{Kn}^3)$ accurate R13 equations, which are obtained by regularizing the G13 equations, incorporate only super-Burnett order terms.

To validate the proposed equations, we first solve Grad's second problem[52,53] and demonstrate that the proposed higher-order transport equations successfully reproduce the Fourier's law [Eq. (47)]. Thereafter, we quantitatively establish that the proposed set of moment equations captures small deviations from the continuum approximation when using Maxwell's molecules (Fig. 2). Furthermore, in agreement with the exact solution of Grad's second problem by using the Boltzmann equation and employing Maxwell molecules,[55] we establish that the proposed moment equations also yield a uniform pressure field and vanishing viscous stresses as all third-order terms vanish in Eq. (46). It should be noted that the R13 equations yield three-dimensional pressure, stress, and temperature

fields due to $\mathcal{O}(\mathrm{Kn}^3)$ contributions that persist in the heat flux equation,[53] while the conventional Burnett and BGK-Burnett equations also result in nonzero shear stress.[52,53]

Next, we utilize the semi-linearized form of the proposed equations to solve the force-driven plane Poiseuille flow problem. In this case, due to the absence of third-order non-linear terms, an equitable comparison can be made with the second-order accurate G13 equations. It is noteworthy that the solutions obtained with the semi-linearized form of the proposed set of equations contain hyperbolic cosine and sine functions in addition to other terms obtained by using the conventional N–S or G13 equations. As demonstrated earlier,[32] such hyperbolic terms are responsible for capturing near-wall Knudsen layer effects that elude the G13 equations. Furthermore, the non-Fourier heat flux in the axial direction $\tilde{q}_1$ that eludes the G13 equations is also captured well with the proposed equations. However, the results from the proposed equations have not been compared with those from the Burnett equations in this paper because no solutions have been reported in the literature. Therefore, no conclusions can be drawn about the superiority of the proposed equations compared to the Burnett equations.

VII. CONCLUSIONS

This paper presents a complete derivation of the second- and third-order representations of the single-particle distribution function at the Burnett level, along with the corresponding closed-form 13-moment transport equations. In comparison to earlier works, the proposed second-order accurate representations form a more concise and manageable system of equations. Furthermore, the proposed third-order accurate moment system contains a larger number of higher-order nonlinear terms from both the second and third order as compared to the G13 equations, thereby allowing non-equilibrium phenomena eluding the G13 equations to be better captured. To validate the proposed moment equations, we present the solutions of Grad's second and the force-driven plane Poiseuille flow problems. We find that the results for Grad's second problem's are consistent with the analytical solution of the Boltzmann equation as well as DSMC simulation results, while those for the plane Poiseuille flow problem are consistent with DSMC results and can capture near-wall Knudsen layer effects. Finally, the entropy generation function has been evaluated for the two considered test cases to demonstrate that the proposed moment equations comply with the second law of thermodynamics.

AUTHOR DECLARATIONS

Conflict of Interest

The authors have no conflicts to disclose.

Author Contributions

U.Y. and A.J. contributed equally in the derivation and formal analyses, while A.A. devised the methodology used in this paper. U.Y., A.J., and A.A. were equally involved in the writing (original draft, review and editing) of this manuscript.

Upendra Yadav: Conceptualization (equal); Formal analysis (equal); Validation (equal); Writing – original draft (equal); Writing – review & editing (equal). **Anirudh Jonnalagadda**: Conceptualization (equal); Formal analysis (equal); Validation (equal); Writing – original draft (equal); Writing – review & editing (equal). **Amit Agrawal**: Project administration (equal); Supervision (equal); Writing – original draft (equal); Writing – review & editing (equal).

DATA AVAILABILITY

The data that support the findings of this study are available from the corresponding author upon reasonable request.

REFERENCES

[1] S. Chapman, T. G. Cowling, and D. Burnett, *The Mathematical Theory of Non-Uniform Gases: An Account of the Kinetic Theory of Viscosity, Thermal Conduction and Diffusion in Gases* (University Press, Cambridge, 1970).
[2] C. Cercignani, *Theory and Application of the Boltzmann Equation* (Scottish Academic Press, 1975).
[3] Y. Sone, "Flows induced by temperature fields in a rarefied gas and their ghost effect on the behavior of a gas in the continuum limit," Annu. Rev. Fluid. Mech. **32**, 779–811 (2000).
[4] A. Agrawal, "A comprehensive review on gas flow in microchannels," Int. J. Micro-Nano Scale Transp. **2**, 1–40 (2011).
[5] A. Akintunde and A. Petculescu, "Infrasonic attenuation in the upper mesosphere–lower thermosphere: A comparison between Navier–Stokes and Burnett predictions," J. Acoust. Soc. Am. **136**, 1483–1486 (2014).
[6] M. S. Ivanov and S. F. Gimelshein, "Computational hypersonic rarefied flows," Annu. Rev. Fluid Mech. **30**, 469 (1998).
[7] M. Gad-el-Hak, "The fluid mechanics of microdevices—The Freeman scholar lecture," J. Fluids Eng. **121**, 5–33 (1999).
[8] E. B. Arkilic, M. A. Schmidt, and K. S. Breuer, "Gaseous slip flow in long microchannels," J. Microelectromech. Syst. **6**, 167–178 (1997).
[9] N. Dongari, A. Agrawal, and A. Agrawal, "Analytical solution of gaseous slip flow in long microchannels," Int. J. Heat Mass Transfer **50**, 3411–3421 (2007).
[10] A. Agrawal, H. M. Kushwaha, and R. S. Jadhav, *Microscale Flow and Heat Transfer* (Springer, 2020).
[11] M. Torrilhon, "Modeling nonequilibrium gas flow based on moment equations," Annu. Rev. Fluid. Mech. **48**, 429–458 (2016).
[12] R. S. Jadhav, N. Singh, and A. Agrawal, "Force-driven compressible plane Poiseuille flow by Onsager-Burnett equations," Phys. Fluids **29**, 102002 (2017).
[13] H. Grad, "On the Kinetic theory of rarefied gases," Commun. Pure Appl. Math. **2**, 331–407 (1949).
[14] I. Müller and T. Ruggeri, *Rational Extended Thermodynamics* (Springer Science & Business Media, 2013), Vol. 37.
[15] D. Burnett, "The distribution of molecular velocities and the mean motion in a non-uniform gas," Proc. London Math. Soc. **s2-40**, 382–435 (1936).
[16] M. S. Shavaliyev, "Super-Burnett corrections to the stress tensor and the heat flux in a gas of Maxwellian molecules," J. Appl. Math. Mech. **57**, 573–576 (1993).
[17] A. Bobylev, "The Chapman-Enskog and Grad methods for solving the Boltzmann equation," Akad. Nauk SSSR Dokl. **262**, 71–75 (1982).
[18] X. Zhong, R. W. MacCormack, and D. R. Chapman, "Stabilization of the Burnett equations and application to hypersonicflows," AIAA J. **31**, 1036–1043 (1993).
[19] L. S. García-Colín, R. M. Velasco, and F. J. Uribe, "Beyond the Navier–Stokes equations: Burnett hydrodynamics," Phys. Rep. **465**, 149–189 (2008).
[20] R. K. Agarwal and R. Balakrishnan, "Numerical simulation of BGK-Burnett equations," Technical Report No. ADA326201 (Wichita State University, Kansas, 1996).
[21] R. Balakrishnan, "An approach to entropy consistency in second-order hydrodynamic equations," J. Fluid Mech. **503**, 201–245 (2004).
[22] R. K. Agarwal, K.-Y. Yun, and R. Balakrishnan, "Beyond Navier–Stokes: Burnett equations for flows in the continuum–transition regime," Phys. Fluids **13**, 3061–3085 (2001).
[23] S. K. Dadzie, "A thermo-mechanically consistent Burnett regime continuum flow equation without Chapman–Enskog expansion," J. Fluid Mech. **716**, 6 (2013).

[24]W. Zhao, W. Chen, and R. K. Agarwal, "Formulation of a new set of simplified conventional Burnett equations for computation of rarefied hypersonic flows," Aerosp. Sci. Technol. **38**, 64–75 (2014).
[25]N. Singh and A. Agrawal, "The Burnett equations in cylindrical coordinates and their solution for flow in a microtube," J. Fluid Mech. **751**, 121–141 (2014).
[26]D. Reitebuch and W. Weiss, "Application of high moment theory to the plane Couette flow," Continuum Mech. Thermodyn. **11**, 217–225 (1999).
[27]D. Risso and P. Cordero, "Dilute gas Couette flow: Theory and molecular dynamics simulation," Phys. Rev. E **56**, 489 (1997).
[28]J. C. Padrino, J. E. Sprittles, and D. A. Lockerby, "Efficient simulation of rarefied gas flow past a particle: A boundary element method for the linearized G13 equations," Phys. Fluids **34**, 062011 (2022).
[29]W. Marques, Jr., G. M. Kremer, and F. M. Sharipov, "Couette flow with slip and jump boundary conditions," Continuum Mech. Thermodyn. **12**, 379–386 (2000).
[30]W. Weiss, "Continuous shock structure in extended thermodynamics," Phys. Rev. E **52**, R5760 (1995).
[31]H. Struchtrup and M. Torrilhon, "Regularization of Grad's 13 moment equations: Derivation and linear analysis," Phys. Fluids **15**, 2668–2680 (2003).
[32]P. Taheri, M. Torrilhon, and H. Struchtrup, "Couette and Poiseuille microflows: Analytical solutions for regularized 13-moment equations," Phys. Fluids **21**, 017102 (2009).
[33]X.-J. Gu and D. R. Emerson, "A high-order moment approach for capturing non-equilibrium phenomena in the transition regime," J. Fluid Mech. **636**, 177–216 (2009).
[34]H. Struchtrup and P. Taheri, "Macroscopic transport models for rarefied gas flows: A brief review," IMA J. Appl. Math. **76**, 672–697 (2011).
[35]X. J. Gu, D. R. Emerson, and G. H. Tang, "Analysis of the slip coefficient and defect velocity in the Knudsen layer of a rarefied gas using the linearized moment equations," Phys. Rev. E **81**, 016313 (2010).
[36]N. Singh and A. Agrawal, "Onsager's-principle-consistent 13-moment transport equations," Phys. Rev. E **93**, 063111 (2016).
[37]N. Singh, R. S. Jadhav, and A. Agrawal, "Derivation of stable Burnett equations for rarefied gas flows," Phys. Rev. E **96**, 013106 (2017).
[38]Y. Zohar, S. Y. K. Lee, W. Y. Lee, L. Jiang, and P. Tong, "Subsonic gas flow in a straight and uniform microchannel," J. Fluid Mech. **472**, 125–151 (2002).
[39]H. Grad, "Principles of the Kinetic theory of gases," in *Thermodynamik der Gase/Thermodynamics of Gases* (Springer, 1958), pp. 205–294.
[40]L. Onsager, "Reciprocal relations in irreversible processes. I," Phys. Rev. **37**, 405 (1931).
[41]L. Onsager, "Reciprocal relations in irreversible processes. II," Phys. Rev. **38**, 2265 (1931).
[42]A. K. Mahendra and R. K. Singh, "Onsager reciprocity principle for kinetic models and kinetic schemes," arXiv:1308.4119 (2013).
[43]A. Jonnalagadda, A. Sharma, and A. Agrawal, "Onsager-regularized lattice Boltzmann method: A nonequilibrium thermodynamics-based regularized lattice Boltzmann method," Phys. Rev. E **104**, 015313 (2021).
[44]R. Balakrishnan, R. K. Agarwal, and K.-Y. Yun, "BGK-Burnett equations for flows in the continuum-transition regime," J. Thermophys. Heat Transfer **13**, 397–410 (1999).
[45]R. S. Jadhav and A. Agrawal, "Strong shock as a stringent test for Onsager-Burnett equations," Phys. Rev. E **102**, 063111 (2020).
[46]R. S. Jadhav and A. Agrawal, "Shock structures using the OBurnett equations in combination with the Holian conjecture," Fluids **6**, 427 (2021).
[47]F. McCourt, J. Beenakker, W. Köhler, and I. Kuščer, *Nonequilibrium Phenomena in Polyatomic Gases, Vol. 2* (Clarendon, Oxford, 1991), Vol. 14, pp. 230–236.
[48]S. R. De Groot and P. Mazur, *Non-Equilibrium Thermodynamics* (Courier Corporation, 2013).
[49]H. Cheng, C. Lee, E. Wong, and H. Yang, "'*Hypersonic slip flows' and issues on extending continuum model beyond the Navier–Stokes level*," in *24th Thermophysics Conference* (AIAA, 1989), p. 1663.
[50]C. Truesdell and R. G. Muncaster, *Fundamentals of Maxwel's Kinetic Theory of a Simple Monatomic Gas: Treated as a Branch of Rational Mechanics* (Academic Press, 1980).
[51]M. Y. Timokhin, H. Struchtrup, A. A. Kokhanchik, and Y. A. Bondar, "Different variants of R13 moment equations applied to the shock-wave structure," Phys. Fluids **29**, 037105 (2017).
[52]R. S. Jadhav and A. Agrawal, "Grad's second problem and its solution within the framework of Burnett hydrodynamics," J. Heat Transfer **142**, 102105 (2020).
[53]R. S. Jadhav and A. Agrawal, "Evaluation of Grad's second problem using different higher order continuum theories," J. Heat Transfer **143**, 012102 (2021).
[54]M. A. Gallis, J. Torczynski, and D. Rader, "Molecular gas dynamics observations of Chapman-Enskog behavior and departures therefrom in nonequilibrium gases," Phys. Rev. E **69**, 042201 (2004).
[55]E. S. Asmolov, N. K. Makashev, and V. I. Nosik, "Heat transfer between plane parallel plates in a gas of Maxwellian molecules," Akad. Nauk SSSR Dokl. **249**, 577–580 (1979).
[56]J. M. Montanero, M. Alaoui, A. Santos, and V. Garzó, "Monte Carlo simulation of the Boltzmann equation for steady Fourier flow," Phys. Rev. E **49**, 367 (1994).
[57]A. Rath, U. Yadav, and A. Agrawal, "Analytical solution of the Burnett equations for gaseous flow in a long microchannel," J. Fluid Mech. **912**, A53 (2021).
[58]A. Rath, N. Singh, and A. Agrawal, "A perturbation-based solution of Burnett equations for gaseous flow in a long microchannel," J. Fluid Mech. **844**, 1038–1051 (2018).
[59]R. Balakrishnan, *Entropy Consistent Formulation and Numerical Simulation of the BGK-Burnett Equations for Hypersonic Flows in the Continuum-Transition Regime* (Wichita State University, 1999).
[60]R. W. Carr, "Quantifying non-equilibrium in hypersonic flows using entropy generation," Ph.D. thesis, Air Force Institute of Technology, 2007.
[61]O. Ejtehadi, J. A. Esfahani, and E. Roohi, "Compressibility and rarefaction effects on entropy and entropy generation in micro/nano Couette flow using DSMC," J. Phys.: Conf. Ser. **362**, 012008 (2012).
[62]W. Welder, D. Chapman, and R. Maccormack, "Evaluation of various forms of the Burnett equations," in *23rd Fluid Dynamics, Plasmadynamics, and Lasers Conference* (AIAA, 1993), p. 3094.